Active Control of Alfven Eigenmodes by Externally Applied 3D Magnetic Perturbations

Active Control of Alfvén Eigenmodes
by Externally Applied 3D Magnetic Perturbations

J. Gonzalez-Martin[1,2],[*] M. Garcia-Munoz[3], J. Galdon-Quiroga[3], Y. Todo[4], J. Dominguez-Palacios[3],
M. Dunne[5], A. Jansen van Vuuren[3], Y.Q. Liu[6], L. Sanchis[7], D. Spong[8], W. Suttrop[5],
X. Wang[5], M. Willensdorfer[5], and the ASDEX Upgrade Team and the Eurofusion MST1 Team

[1]*Department of Mechanical Engineering and Manufacturing,*
University of Seville, Camino de los Descubrimientos s/n, 41092 Seville, Spain
[2]*Department of Physics and Astronomy, University of California, Irvine, California 92697, USA*
[3]*Department of Atomic, Molecular and Nuclear Physics, University of Seville, 41012 Seville, Spain*
[4]*National Institute for Fusion Science, Toki 509-5292, Japan*
[5]*Max Planck Institute for Plasma Physics, Boltzmannstrasse, 2 85748 Garching bei Munchen, Germany*
[6]*General Atomics, PO Box 85608, San Diego, CA 92186-5608, USA*
[7]*Department of Applied Physics, Aalto University, FI-00076, Aalto, Finland and*
[8]*Oak Ridge National Laboratory, Oak Ridge, Tennessee 37831*

The suppression and excitation of Alfvén eigenmodes have been experimentally obtained, for the first time, by means of externally applied 3D perturbative fields with different spatial spectra in a tokamak plasma. The applied perturbation causes an internal fast-ion redistribution that modifies the phase-space gradients responsible for driving the modes, determining, ultimately their existence. Hybrid kinetic-magnetohydrodynamic simulations reveal an edge resonant transport layer activated by the 3D perturbative field as the responsible mechanism for the fast-ion redistribution. The results presented here may help to control fast-ion driven Alfvénic instabilities in future burning plasmas with a significant fusion born alpha particle population.

Introduction.— Alfvén waves are electromagnetic fluctuations inherent to a wide variety of laboratory and space plasmas [1]. Their interaction with charged particles can lead to a net wave-particle energy exchange with dramatic consequences for the surroundings. In space plasmas, for instance, kinetic Alfvén waves play a key role in the heating of the solar corona [2, 3], generation of the fast solar wind [4, 5], and propagation of cosmic rays in the interstellar space [6, 7]. On Earth, Alfvén waves are routinely observed on magnetically confined fusion devices with a significant population of energetic particles [8, 9]. Indeed, phase-space gradients in the energetic particle distribution constitute an essential source of energy that can destabilize a rich spectrum of Alfvén eigenmodes (AEs). If not properly abated, AEs can lead to a radial energetic particle transport in tokamaks and stellarators that can compromise the realisation of magnetically confined fusion. External actuators to control the AE activity, and associated energetic particle population, in a magnetically confined fusion device might, thus, be mandatory. In tokamaks, externally applied 3D fields commonly used to suppress Edge Localised Modes (ELMs) [10–12], Resistive Wall Modes (RWMs), lock modes [13, 14], lock modes [15] and have been recently used to mitigate AEs in the NSTX tokamak [16, 17].
In this letter, we show, for the first time, the suppression and excitation of AEs by means of externally applied 3D fields with different spatial spectra. The results presented here open a new avenue to an active AE control in a burning plasma with a significant fusion born alpha particle population by creating internal transport barriers for specific energetic particle populations.

Experiment.—The discharges discussed here were carried out in the ASDEX Upgrade (AUG) tokamak in matched ELMy H-mode plasmas with a toroidal magnetic field on axis of $B_t = 2.5$ T, a plasma current $I_p = 0.6$ MA, a normalized ratio of plasma pressure to magnetic pressure of $\beta_N = 1.2$ and low collisionallity ($\nu_e^* \approx 0.2$). Traces of these discharges are depicted in Fig. 1. 1.5 MW of on-axis counter Electron Cyclotron Current Drive (ECCD) (figure 1a) together with two sources (2.5 MW each) of early Neutral Beam Injection (NBI) produced an elevated q-profile. Two tangential sources are applied since the beginning of the discharge, until one of the sources is replaced by a radial one at 3.0 s. Resonant Magnetic Perturbations (RMPs) with toroidicity $n = 2$ are applied by two sets of eight ELM control coils, one above the midplane and one below [18]. The poloidal spectrum of the applied perturbation is tuned by rotating the phase of the upper set (ϕ_U) while fixing the lower (ϕ_L), inducing a phase shift between both coil sets ($\Delta\phi_{UL} = \phi_U - \phi_L$). Figure 1 (b) shows how consecutive RMP blips of 200 ms are applied in two comparable discharges (figure 1 (b)) whose main difference is the applied coil phasing, previously selected by scanning $\Delta\phi_{UL}$ to maximize ($\Delta\varphi_{UL} = 100°$) and minimize ($\Delta\varphi_{UL} = -50°$) the signal on the fast-ion loss detector (FILD) [19]. Figure 1(c) illustrates how the same line integrated densities are measured in both discharges. The same density pump out is produced by both poloidal spectrums, giving confidence that the neutral beam deposition profile is not affected by the coil phasing of the applied perturbation. In these two pulses, the ELMs are mitigated to half of their natural amplitude regardless
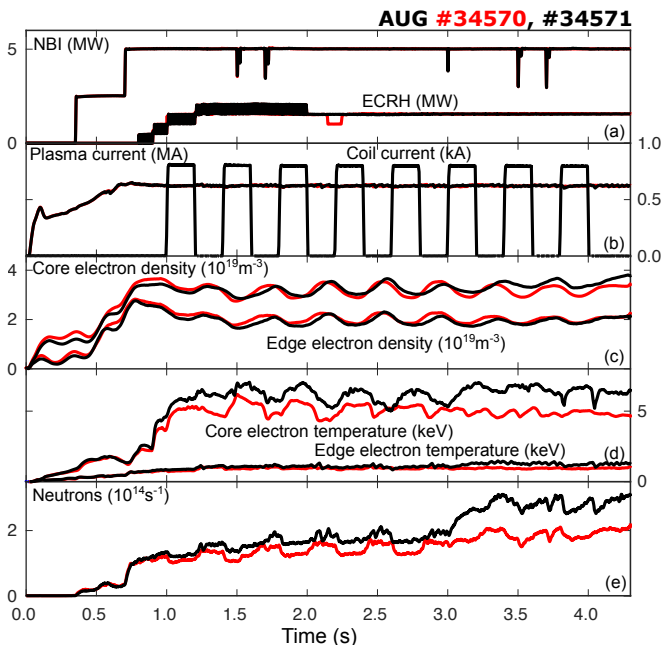
FIG. 1. Temporal evolution of (a) auxiliary heating, (b) plasma and ELM control current, (c) electron density, (d) electron temperature, and (e) neutron flux. Black and blue traces correspond to discharges #34570 and #34571 respectively, where MP pulses with coil phasing $\Delta\varphi_{UL} = 100°$ and $\Delta\varphi_{UL} = -50°$ are applied.

FIG. 2. Color-coded spectrogram showing TAE activity in the range n=2-5. Overplayed white traces represent the MP coil current with coil phasing $\Delta\varphi_{UL} = 100°$ (a) and $\Delta\varphi_{UL} = -50°$ (b). Temporal evolution of the fast-ion losses measured by the FILD diagnostic (c).

the poloidal spectrum of the applied perturbation. On the other hand, despite the fact that figure 1 (d) shows that electron temperature is sightly higher on discharge #34571 before the RMPs pulses are applied (attributed to a small difference in wall conditioning / recycling), it is clear that the same relative variation on the temperature profile is induced by the MP pulses in both discharges. Similar behaviour is reflected on the measured neutron yield (figure 1 (e)), revealing that the applied MPs produce the same level of global fast-ion (FI) redistribution in both discharges.

During the flattop phase, the suprathermal population of deuterium ions injected by the NBI destabilizes different branches of Alfvén eigenmodes, including Toroidicity-induced AEs (TAEs) with frequencies $80-110$ kHz and toroidal mode numbers $n=2-5$. The amplitude evolution of these modes is depicted on the Mirnov coil spectrograms in figure 2 (a) and (b) for coil phasing $\Delta\varphi_{UL} = 100°$ and $\Delta\varphi_{UL} = -50°$ respectively. NBI blips on similar discharges reveal that a fully relaxed FI slowed-down distribution is needed to overcome marginal stability, confirming that the mode drive of these low frequency Alfvén instabilities is dominated by the fast-ion spatial gradient.

As soon as the RMP blips with $\Delta\varphi_{UL} = 100°$ are applied, the TAEs are clearly mitigated. Later in time, as the safety factor relaxes producing TAEs closer to marginal stability and the tangential beam source is re-
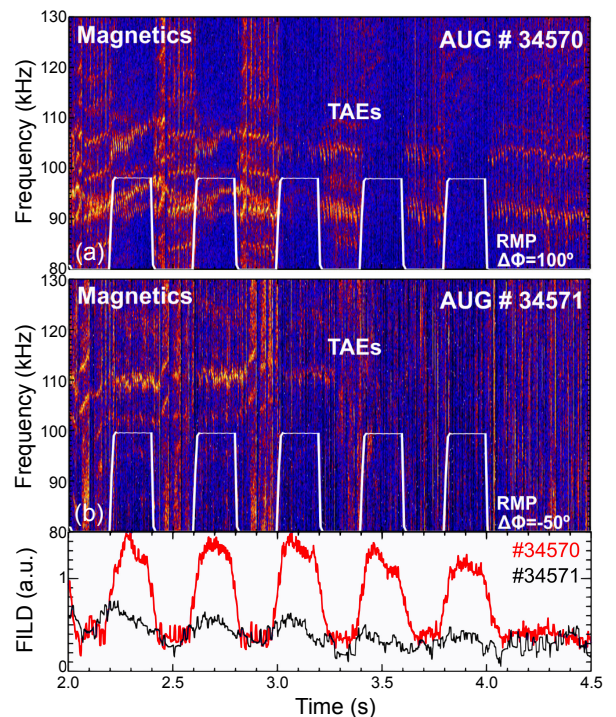
placed by a radial one, the RMP blips achieve a full suppression of the TAEs. An abrupt increase in the fast channel of the fast-ion loss detector is observed each time this coil phasing is applied, as depicted in figure 2 (c). On shot #34571, contrarily, the TAEs are virtually not observed when the RMPs are not applied due to the slightly higher radiative damping induced by the larger electron temperature. When the RMP blips of $\Delta\varphi_{UL} = -50°$ are applied, the FILD signal suffers a much smaller increase and the TAEs are amplified becoming visible on the spectrogram of the Mirnov coil signal. This enhancing effect induced by the $\Delta\varphi_{UL} = -50°$ MP blips indicate an increase in the fast-ion drive with respect to the poloidal spectrum applied by the $\Delta\varphi_{UL} = 100°$ MP blips. This complete control of the TAE amplitude occurs within $\sim$ 0.1 ms, a typical orbital time scale. In contrast, when the RMP blips are turned off, the bursting persists, at sighly smaller amplitude for several milliseconds, indicating the collisional time scale that the entire fast-ion distribution function needs to evolve.

Signature of internal phase-space redistribution.— Figure 3 (a) shows the velocity-space pattern measured by the FILD diagnostic. One can identify the injected full and half energies, ELM-induced high energy tail [20] induced by the tangential source and an additional spot that corresponds to the injected main energy of the ra-
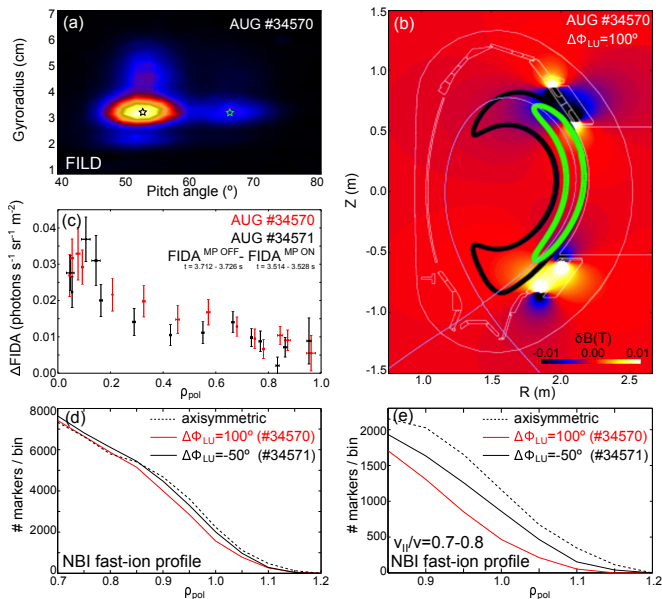
FIG. 3. (a) Velocity-space pattern of the measured losses when MP are active. (b) Poloidal projection of the trajectory of the measured lost ions overlapping the imposed MP fields. (c) MP induced drop on the fast-ion profile measured by FIDA. Integrated (d) and pitch-filtered (e) FI radial profile simulated with the ASCOT code for both coil phasing.

dial source. Figure 3 (b) shows the poloidal projection of the FI orbits of the MP-induced spot and prompt losses captured by FILD. These spots correspond to trapped orbits that explore the applied MP fields on their outer banana leg. The shape of the measured velocity-space pattern is identical in both discharges, indicating that the same geometrical resonances are responsible of the FI radial transport for both coil phasing. This agrees with previous experimental and numerical investigations on the edge resonant transport layer (ERTL) [21] that explain how an injected FI might suffer inward and outward transport depending upon the applied poloidal spectrum. Unlike the shape of the velocity-space pattern of the losses, as shown in figure 2 (a), the magnitude of the fast-ion flux of the measured velocity-space is strongly affected by the applied coil phasing. This variation of the measured fast-ion flux can be interpreted as a signature of the internal FI redistribution in phase-space. This redistribution is strongly dependent on the particle orbit, given by its energy and local pitch angle, and hence cannot be captured by diagnostics that integrate over a large region of velocity-space such as neutron detector or fast-ion D_α (FIDA) spectroscopy [22]. Indeed, as shown in figure 1 (e), the neutron flux decays identically in both discharges independently of the applied coil phasing. Similar observations are performed by the FIDA diagnostic: Figure 3 (c) depicts the measured level of FI drop induced by the MPs, which is larger at the core due to the higher FI density. One can observe that

the FI drop induced by the MPs is within the error bars for both coil phasing along the entire minor radius.

Modelling.— The impact of the MP fields on the fast-ion population is investigated by employing the full-orbit ASCOT code [23], which includes a realistic NBI birth profile, collisions, a 3D wall for numerical particles and has been validated against FI diagnostics on multiple occasions [21, 24, 25]. The radial profile of the resulting steady state FI distribution function is depicted in figure 3 (d) for both coil phasing and without MPs. A small and similar FI drop is found for both coil phasing, being the one induced by $\Delta\varphi_{UL} = 100°$ higher by a very small amount, in agreement with the inferred drop in the global FI profiles captured by FIDA. On the other hand, figure 3 (e) shows the FI radial profiles calculated by ASCOT, including only the particles with a pitch angle in a small range around the pitch injected by the NBI source and captured by the FILD diagnostic. A more significant difference is found to be induced by the applied coil phasing at the edge of these pitch-filtered profiles, explaining the observed effect that the applied poloidal spectrum has on the FI loss flux measured by FILD (figure 2 (c)). The difference between pitch-filtered and pitch-integrated profiles confirms that the MP-induced redistribution has a velocity-space localized nature, clearly captured by FILD, yet blurred on the global FIDA and neutron flux measurements.

The 3D non-linear hybrid kinetic-magnetohydrodynamic (MHD) MEGA code [26–29] is employed to understand the underlying mechanisms connecting the internal velocity-space localised FI redistribution induced by the MPs and the dependence of the TAE amplitude on the applied poloidal spectrum. Figure 4 (a) depicts the measured electron density and temperature profiles that are employed in the simulations, together with the safety factor of the CLISTE equilibrium reconstruction [30] used as the initial condition for the electromagnetic background. The equilibrium has a reversed shear with two $q = 3$ rational surfaces at normalized minor radius $\rho_{pol} = 0.3$ and $\rho_{pol} = 0.5$ constrained by MHD markers and motional stark effect (MSE) measurements. The magnetic shear is significant in the region $\rho_{pol} > 0.6$. Figure 4 (b) shows the space-integrated velocity-space of the anisotropic slowing-down FI distribution (similar to [31–33]) employed in the simulation. This model captures the main features of the distribution calculated by the NUBEAM module of TRANSP [34]. TAEs are destabilized in the same $n=2-5$ range observed in the experiment, propagating along the ion-diamagnetic drift direction and saturating within ≈ 0.1 ms. The radial location and frequency of one of these TAEs ($n=4$) is depicted on the shear Alfvén wave continuum in figure 4 (c), showing that the mode is located in the TAE gap at the same frequency as observed in the experiment. These simulations also reproduce the radial
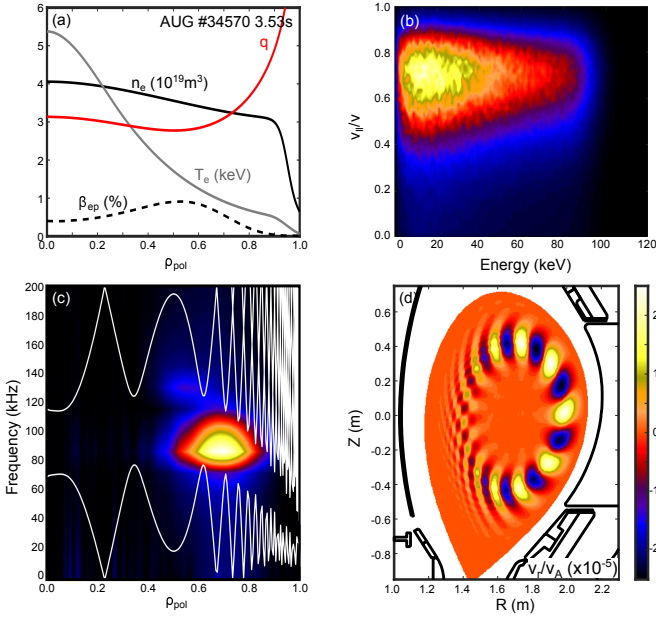
FIG. 4. (a) Kinetic profiles and safety factor inferred from the experiment and employed on the MEGA simulation (b) Space-integrated velocity-space of the employed anisotropic slowing down FI distribution employed in MEGA. (c) Location of the simulated TAE on the shear Alvén wave continuum. (d) Poloidal structure of the simulated TAE.

FIG. 5. For particles with magnetic moment $\mu = 2 \times 10^{-15} \text{kgm}^2\text{s}^{-2}\text{T}^{-1}$, ERTL induced by MPs for coil phasing $\Delta\varphi_{UL} = 100°$ (a) and $\Delta\varphi_{UL} = -50°$ (b) producing a modification of the total gradient. Predicted particle-wave energy exchange based on gradients of the FI distribution (c) and simulated by MEGA (d) both overlaying the ERTL location.

location of $\rho_{pol} \approx 0.7$ observed by the electron cyclotron emission diagnostic (ECE)[35] and the frequency of the toroidal harmonics observed in the experiment. Figure 4 (d) shows the poloidal structure of the radial velocity associated with the instability, which, as to the toroidal electric field, has the expected ballooning structure.

The externally applied 3D fields are superimposed to the same axisymmetric background before the MHD force balance is calculated as the initial simulation time-step. As a result, the TAEs are destabilized in a steady 3D background. The resulting mode frequency, location and poloidal structure are not affected by the 3D fields. However, the growth rates are dependent on the applied coil phasing, producing $\Delta\varphi_{UL} = -50°$ a slightly higher linear growth rate than $\Delta\varphi_{UL} = 100°$, in line with the trend observed in the experiment. The inclusion of plasma response to the externally applied 3D fields does not modify the obtained growth rate of the modes.

MEGA calculates the particle-wave energy exchange during the linear phase of the destabilized TAEs, which is found to be located in the vicinity of magnetic moment $\mu = 2 \times 10^{-15} \text{kgm}^2\text{s}^{-2}\text{T}^{-1}$. ASCOT simulations are employed to visualize how the ERTL affect those particles without the presence of TAEs. To do that, μ is kept fixed while the motion invariants energy (E) and toroidal canonical momentum (P_ϕ) are varied, being $P_\phi = Ze\psi + mRv_\phi$, with Ze the particle charge, ψ the poloidal flux, m the particle mass, R the major ra-
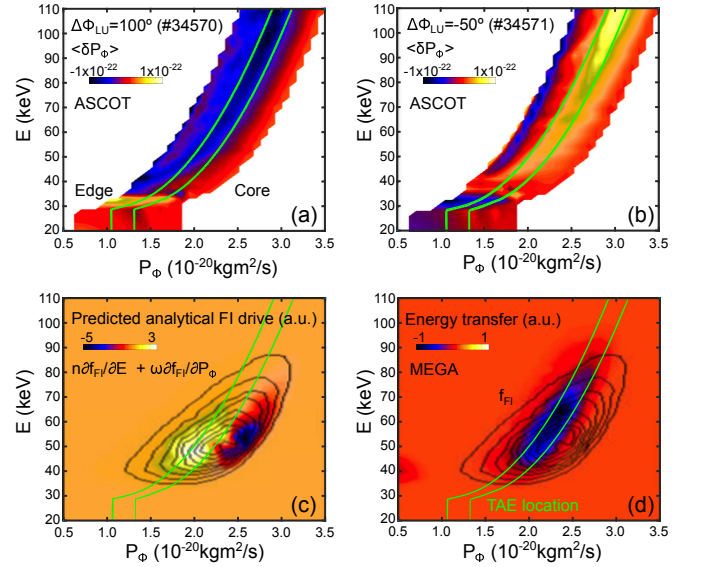
dius and v_ϕ the toroial projection of the particle velocity. The time-integrated variation of the toroidal canonical momentum $< \delta P_\phi >$ is depicted for both coil phasing in figures 5 (a) and (b). The green lines represent the particles that overlap the TAEs when crossing the midplane upwards. The particles overlapping both TAE and ERTL suffer from a $< \delta P_\phi >$ of $\approx 1\%$, big enough to induce an internal redistribution affecting the P_ϕ gradients, but too small to reach the plasma edge. One can conclude that particles captured by FILD are initially closer to the plasma edge, not exploring the TAE, explaining the fact that FILD does not measure coherent losses at the frequency of those TAEs.

The mode drive (and damping), γ_{TAE}, induced by FI can be located in phase-space beforehand by taking the gradients of the fast-ion distribution function (f_{FI}) as follows,

$$\gamma_{TAE} \sim n \frac{\partial f_{FI}}{\partial P_\phi} + \omega \frac{\partial f_{FI}}{\partial E}. \tag{1}$$

The predicted drive for the simulated instabilities is depicted in figure 5 (c) and the calculated energy transfer during the linear phase of the hybrid simulation in figure 5 (d). The solid black lines represent the FI distribution for the selected μ. Both predicted and simulated energy exchange show the same location on phase-space (about 60 keV), giving confidence on the result. This fast-ion drive is observed to overlap the ERTL location. The $< \delta P_\phi >$ induced at the phase-space region driving the TAEs by the MPs with $\Delta\varphi_{UL} = 100°$ is negative,

producing a local flattering of the FI distribution, while MPs with $\Delta\varphi_{UL} = -50°$ are positive, increasing the gradient and therefore the drive. This explains why the MP can cause a general loss of FI confinement measured by neutrons and FIDA, while the applied poloidal spectrum can induce different local re-distributions overlapping the TAE drive, affecting the mode amplitude.

Summary and discussion.— The first experimental evidence of suppression / excitation of the amplitude of TAEs by modifying the poloidal spectrum of the externally applied 3D fields is presented. An identical drop on the global FI signals measured by FIDA and neutron diagnostics is observed regardless the applied coil phasing and TAE amplitude, while different levels on the FI loss flux are recorded at selected velocity-space regions by the FILD diagnostic. These losses are a signature of the ERTL, which induces internal re-distributions of the FI population, that locally modify the P_ϕ gradients of the FI distribution at the phase-space location of the TAE drive. In devices such as ITER that will already employ externally applied 3D perturbations to suppress ELMs and other detrimental instabilities, this mechanism might trigger AEs causing a loss of confinement, while small modifications on the applied poloidal spectrum could reverse this effect, locally relaxing the FI gradients, and therefore suppressing the AEs. This phase-space engineering technique opens the door to a AE-induced transport suppression that might be employed to improve the confinement of both alphas and injected beam ions, while maintaining the same level of pedestal degradation and ELM suppression in future burning plasmas.

————————

* jgonzalez62@us.es

[1] H. Alfvén. *Nature*, 150:405–406, 10 1942.

[2] S. Tomczyk, S. W. McIntosh, S. L. Keil, P. G. Judge, T. Schad, D. H. Seeley, and J. Edmondson. *Science*, 317(5842):1192–1196, 2007.

[3] S. R. Cranmer and A. A. van Ballegooijen. *The Astrophysical Journal*, 594:573–591, 9 2003.

[4] J. W. Cirtain, L. Golub, L. Lundquist, A. Van Ballegooijen, A. Savcheva, M. Shimojo, E. DeLuca, S. Tsuneta, T. Sakao, K. Reeves, M. Weber, R. Kano, N. Narukage, and K. Shibasaki. *Science*, 318:1580–1582, 12 2007.

[5] A. Hasegawa. *Journal of Geophysical Research*, 81(28):5083–5090, 1976.

[6] Katia M. Ferrière. *Rev. Mod. Phys.*, 73:1031–1066, Dec 2001.

[7] Russell Kulsrud and William P. Pearce. *ApJ*, 156:445, 5 1969.

[8] K. L. Wong, R. J. Fonck, S. F. Paul, D. R. Roberts, E. D. Fredrickson, R. Nazikian, H. K. Park, M. Bell, N. L. Bretz, R. Budny, S. Cohen, G. W. Hammett, F. C. Jobes, D. M. Meade, S. S. Medley, D. Mueller, Y. Nagayama, D. K. Owens, and E. J. Synakowski. *Physical Review Letters*, 66:1874, 4 1991.

[9] W. W. Heidbrink, E. J. Strait, E. Doyle, G. Sager, and R. T. Snider. *Nuclear Fusion*, 31:1635, 9 1991.

[10] T. E. Evans, R. A. Moyer, K. H. Burrell, M. E. Fenstermacher, I. Joseph, A. W. Leonard, T. H. Osborne, G. D. Porter, M. J. Schaffer, P. B. Snyder, P. R. Thomas, J. G. Watkins, and W. P. West. *Nature Physics*, 2:419–423, 5 2006.

[11] A. Loarte. *Nature Physics*, 2:369–370, 2006.

[12] W. Suttrop, T. Eich, J. C. Fuchs, S. Günter, A. Janzer, A. Herrmann, A. Kallenbach, P. T. Lang, T. Lunt, M. Maraschek, R. M. McDermott, A. Mlynek, T. Pütterich, M. Rott, T. Vierle, E. Wolfrum, Q. Yu, I. Zammuto, and H. Zohm. *Physical Review Letters*, 106(22):225004, 2011.

[13] Y. Q. Liu and A. Bondeson. *Physical Review Letters*, 84:907, 1 2000.

[14] S. A. Sabbagh, R. E. Bell, J. E. Menard, D. A. Gates, A. C. Sontag, J. M. Bialek, B. P. LeBlanc, F. M. Levinton, K. Tritz, and H. Yuh. *Physical Review Letters*, 97:045004, 7 2006.

[15] T. C. Hender, R. Fitzpatrick, A. W. Morris, P. G. Carolan, R. D. Durst, T. Edlington, J. Ferreira, S. J. Fielding, P. S. Haynes, J. Hugill, I. J. Jenkins, R. J. La Haye, B. J. Parham, D. C. Robinson, T. N. Todd, M. Valovic, and G. Vayakis. *Nuclear Fusion*, 32:2091, 12 1992.

[16] A. Bortolon, W. W. Heidbrink, G. J. Kramer, J. K. Park, E. D. Fredrickson, J. D. Lore, and M. Podestà. *Physical Review Letters*, 110(26):265008, 2013.

[17] G. J. Kramer, A. Bortolon, N. M. Ferraro, D. A. Spong, N. A. Crocker, D. S. Darrow, E. D. Fredrickson, S. Kubota, J. K. Park, M. Podestà, W. W. Heidbrink, and the NSTX Team. *Plasma Physics and Controlled Fusion*, 58(8):085003, 2016.

[18] W. Suttrop, O. Gruber, S. Günter, D. Hahn, A. Herrmann, M. Rott, T. Vierle, U. Seidel, M. Sempf, B. Streibl, E. Strumberger, D. Yadikin, O. Neubauer, B. Unterberg, E. Gaio, V. Toigo, and P. Brunsell. *Fusion Engineering and Design*, 84(2-6):290–294, 2009.

[19] M. García-Muñoz, H.-U. Fahrbach, and H. Zohm. *Review of Scientific Instruments*, 80:053503, 5 2009.

[20] J. Galdon-Quiroga, M. Garcia-Munoz, K. G. McClements, M. Nocente, M. Hoelzl, A. S. Jacobsen, F. Orain, J. F. Rivero-Rodriguez, M. Salewski, L. Sanchis-Sanchez, W. Suttrop, and E. Viezzer. *Physical Review Letters*, 121:025002, 7 2018.

[21] L. Sanchis, M. Garcia-Munoz, A. Snicker, D. A. Ryan, D. Zarzoso, L. Chen, J. Galdon-Quiroga, M. Nocente, J. F. Rivero-Rodriguez, M. Rodriguez-Ramos, W. Suttrop, M. A. Van Zeeland, E. Viezzer, M. Willensdorfer, and F. Zonca. *Plasma Physics and Controlled Fusion*, 61(1):014038, 2019.

[22] W. W. Heidbrink, K. H. Burrell, Y. Luo, N. A. Pablant,

and E. Ruskov. *Plasma Physics and Controlled Fusion*, 46(12):1855–1875, nov 2004.

[23] E. Hirvijoki, O. Asunta, T. Koskela, T. Kurki-Suonio, J. Miettunen, S. Sipilä, A. Snicker, and S. Äkäslompolo. *Computer Physics Communications*, 185:1310–1321, 4 2014.

[24] J. Galdon-Quiroga, M. Garcia-Munoz, L. Sanchis-Sanchez, M. Mantsinen, S. Fietz, V. Igochine, M. Maraschek, M. Rodriguez-Ramos, B. Sieglin, A. Snicker, G. Tardini, D. Vezinet, M. Weiland, L.G. Eriksson, The ASDEX Upgrade Team, and The EUROfusion MST1 Team. *Nuclear Fusion*, 58:036005, 1 2018.

[25] S. Sipilä, J. Varje, T. Johnson, R. Bilato, J. Galdón-Quiroga, A. Snicker, T. Kurki-Suonio, L. Sanchis, D. Silvagni, J. González-Martín, the ASDEX Upgrade Team, and the EUROfusion MST1 Team. *Nuclear Fusion*, 61:086026, 7 2021.

[26] Y. Todo and T. Sato. *Physics of Plasmas*, 5:1321–1327, 1998.

[27] Y. Todo and A. Bierwage. *Plasma and Fusion Research*, 9(0):3403068–3403068, 2014.

[28] Y. Todo, M. A. Van Zeeland, and W. W. Heidbrink. *Nuclear Fusion*, 56:112008, 7 2016.

[29] A. Bierwage, K. Shinohara, Y. Todo, N. Aiba, M. Ishikawa, G. Matsunaga, M. Takechi, and M. Yagi. *Nature Communications*, 9:1–11, 12 2018.

[30] P. J. Mc Carthy. *Physics of Plasmas*, 6:3554, 8 1999.

[31] H. Wang, Y. Todo, and C. C. Kim. *Physical Review Letters*, 110:155006, 4 2013.

[32] M. A. Van Zeeland, L. Bardoczi, J. Gonzalez-Martin, W. W. Heidbrink, M. Podesta, M. Austin, C. S. Collins, X. D. Du, V. N. Duarte, M. Garcia-Munoz, S. Munaretto, K. E. Thome, Y. Todo, and X. Wang. *Nuclear Fusion*, 61:066028, 5 2021.

[33] A. Bierwage, Y. Todo, N. Aiba, and K. Shinohara. *Nuclear Fusion*, 54:104001, 10 2014.

[34] A. Pankin, D. McCune, R. Andre, G. Bateman, and A. Kritz. *Computer Physics Communications*, 159:157–184, 6 2004.

[35] M. A. Van Zeeland, G. J. Kramer, M. E. Austin, R. L. Boivin, W. W. Heidbrink, M. A. Makowski, G. R. McKee, R. Nazikian, W. M. Solomon, and G. Wang. *Physical Review Letters*, 97:1–4, 2006.